AIAA JOURNAL
Vol. 36, No. 6, June 1998

# Technical Notes

*TECHNICAL NOTES are short manuscripts describing new developments or important results of a preliminary nature. These Notes cannot exceed 6 manuscript pages and 3 figures; a page of text may be substituted for a figure and vice versa. After informal review by the editors, they may be published within a few months of the date of receipt. Style requirements are the same as for regular contributions (see inside back cover).*

## Sensitivity Analysis of Nonlinear Material and Its Application to Shape Optimization

Koetsu Yamazaki*
*Kanazawa University, Kanazawa 920, Japan*
and
Kazuhiro Shibuya†
*YHP, Inc., Tokyo 168, Japan*

### Introduction

PERFORMANCE requirements in many industries have frequently necessitated using materials beyond their elastic and linear limits to reduce the cost and weight of structures. Considerable efforts have been made recently to establish the sensitivity analysis technique of nonlinear structures in which path-dependent and path-independent problems have been treated. Early works addressed the design sensitivities and optimal design for the geometrical or material nonlinearity, or both, under monotonous loadings.[1–4] However, this approach seems unattractive from the viewpoint of computational efficiency because the entire response analysis is required to calculate the related sensitivities of response. Cheng and Song[5] first insisted on the necessity of treating sensitivity discontinuity for piecewise linear constitutive law. Recently, Jao and Arora[6] also treated the path-dependent response sensitivities with discontinuity based on the updated Lagrangian formulation and applied to the nonlinear structural optimization. In their method, the design sensitivity equation is given for the total sensitivity instead of its increments at a loading level to avoid treating the discontinuity directly. Ohsaki and Arora[7] also suggested introducing the yielding time concept to treat the sensitivity discontinuity, but the implementation is extremely difficult for complicated problems. Hisada[8] developed an efficient and approximate technique to implement the nonlinear sensitivity calculation; however, the method requires improvement of precision. Furthermore, the sensitivity analysis technique of path-dependent problems has not yet been applied to shape optimization.

In this Note, a direct sensitivity analysis technique for the path-dependent nonlinear problem based on the updated Lagrangian formulation is suggested in which the elastoplastic material of bilinear constitutive law is assumed. For such a material property, the design sensitivities are discontinuous at the material transition points. The incremental equilibrium equation is differentiated with respect to the design variables to derive the sensitivity equations, which are solved during the Newton–Raphson iterative scheme of response analysis. Then the sensitivities of incremental displacement are accumulated to obtain the total sensitivity of displacement at the current load level. The discontinuity of the displacement at the material transition points is overcome directly by using the differentiated form of constitutive equation at the yielding points.

Presented as Paper 95-1364 at the AIAA/ASME/ASCE/AHS/ASC 36th Structures, Structural Dynamics, and Materials Conference, New Orleans, LA, April 10–13, 1995; received Aug. 19, 1996; revision received Feb. 17, 1998; accepted for publication Feb. 23, 1998. 

*Professor, Department of Mechanical Systems Engineering, 2-40-20 Kodatsuno. Member AIAA.
†Engineer, Sales Development Division, 3-29-21 Takaido-higashi, Suginami-ku.

### Sensitivity Analysis of Elastoplastic Materials

#### Newton–Raphson Scheme for Nonlinear Structural Analysis

When the Newton–Raphson iteration scheme is adopted to obtain the incremental displacement, the discrete form of incremental equilibrium equation for the elastoplastic materials at an iterative step $i$ can be written as

$$\boldsymbol{K}^{(i)}\Delta\boldsymbol{u}^{(i)} = \Delta\boldsymbol{F}^{(i)} - \Delta\boldsymbol{R}^{(i-1)} \tag{1}$$

where $\Delta\boldsymbol{u}^{(i)}$ is the displacement at a Newton–Raphson iteration $i$ and $\boldsymbol{K}^{(i)}$ is the incremental stiffness matrix. When we consider the two-dimensional problems, the incremental stiffness is assembled by the element stiffness given by the isoparametric mapping of natural coordinates $\xi$–$\eta$ as

$$\boldsymbol{K}^{(i)} = \sum_e \int_{-1}^{1}\int_{-1}^{1} \boldsymbol{B}^T\boldsymbol{D}\boldsymbol{B}\,|\boldsymbol{J}|\,\mathrm{d}\xi\,\mathrm{d}\eta \tag{2}$$

in which $\boldsymbol{B}$ and $\boldsymbol{D}$ denote the strain-displacement transformation and stress-strain matrices, respectively, and $|\boldsymbol{J}|$ is the Jacobian matrix for mapping. On the other hand, $\Delta\boldsymbol{R}^{(i)}$ is the internal force vector and is assembled by the internal force vector of each element calculated by the total stress increment $\Delta\sigma$ at a load increment as

$$\Delta\boldsymbol{R}^{(i)} = \sum_e \int_{-1}^{1}\int_{-1}^{1} \boldsymbol{B}^T\Delta\sigma\,|\boldsymbol{J}|\,\mathrm{d}\xi\,\mathrm{d}\eta \tag{3}$$

and $\Delta\boldsymbol{R}^{(0)} = \boldsymbol{0}$. Then the total increment of displacement $\Delta\boldsymbol{U}^{(i)}$ at a loading step is updated as

$$\Delta\boldsymbol{U}^{(i)} = \Delta\boldsymbol{U}^{(i-1)} + \Delta\boldsymbol{u}^{(i)} \tag{4}$$

This iterative Newton–Raphson scheme is repeated until the imbalance force of the right-hand side of Eq. (1) becomes zero.

#### Constitutive Law

To treat the elastoplastic material behavior, a bilinear stress–strain relationship and von Mises yield function are assumed in this study. When the plane stress condition is assumed, the von Mises yield function $F$ is expressed in terms of deviatoric stress components $\sigma'_{ij}$ and the Cauchy stress as

$$\begin{gathered} F = \tfrac{3}{2}\sigma'_{ij}\sigma'_{ij} - \sigma_Y^2 = \sigma_x^2 - \sigma_x\sigma_y + \sigma_y^2 + 3\tau_{xy}^2 - \sigma_Y^2 \le 0 \\ \sigma_Y = \sigma_{Y0} + H'\bar{\varepsilon}_p, \qquad H' = EE_T/(E - E_T) \end{gathered} \tag{5}$$

where $\sigma_{Y0}$, $E$, and $E_T$ are the initial yield stress, Young's modulus, and strain-hardening modulus, respectively. The equivalent plastic strain $\bar{\varepsilon}_p$ depends on the plastic strain history and is given by the history-dependent integration.

#### Direct Analysis of Design Sensitivity

By differentiating Newton–Raphson iterative equation (1) with respect to the design variable $b$, the direct differentiation method gives the sensitivity equation of incremental displacement as

$$\boldsymbol{K}^{(i)}\frac{\partial\Delta\boldsymbol{u}^{(i)}}{\partial b} = -\frac{\partial\boldsymbol{K}^{(i)}}{\partial b}\Delta\boldsymbol{u}^{(i)} - \frac{\partial\boldsymbol{R}^{(i)}}{\partial b} \tag{6}$$

The preceding sensitivity equation is solved for each iteration step $i$ during the Newton–Raphson iteration of response. The pseudoload

of the right-hand side of Eq. (6) is evaluated from the sensitivities of the internal load vector and the stiffness matrix given as

$$\frac{\partial \boldsymbol{K}^{(i)}}{\partial b} = \sum_e \int_{-1}^{1}\int_{-1}^{1}\left[\left(\frac{\partial \boldsymbol{B}^T}{\partial b}\boldsymbol{D}\boldsymbol{B} + \boldsymbol{B}^T\frac{\partial \boldsymbol{D}}{\partial b}\boldsymbol{B} + \boldsymbol{B}^T\boldsymbol{D}\frac{\partial \boldsymbol{B}}{\partial b}\right)|\boldsymbol{J}| + \boldsymbol{B}^T\boldsymbol{D}\boldsymbol{B}\frac{\partial |\boldsymbol{J}|}{\partial b}\right] \mathrm{d}\xi\,\mathrm{d}\eta \tag{7}$$

in which the second term, including the derivative of the $\boldsymbol{D}$ matrix, should be evaluated at only Gauss integral points where the stress state is yielding.

On the other hand, we have to reformulate the expression of the internal force vector to take the sensitivity discontinuity at yielding points into consideration. Let us consider a transient process from the elastic state into the plastic one. If a stress increment $\Delta\sigma$ is separated into an elastic component $\Delta\sigma_e$ and a plastic component $\Delta\sigma_p$ ($\Delta\sigma = \Delta\sigma_e + \Delta\sigma_p$), the internal force vector of Eq. (3) is represented as

$$\begin{aligned}\boldsymbol{R}^{(i)} &= \sum_e \int_{-1}^{1}\int_{-1}^{1}\left(\boldsymbol{B}^T\Delta\sigma_e + \boldsymbol{B}^T\Delta\sigma_p\right)|\boldsymbol{J}|\,\mathrm{d}\xi\,\mathrm{d}\eta \\ &= \sum_e \int_{-1}^{1}\int_{-1}^{1}\left(\boldsymbol{B}^T\boldsymbol{D}_e R\Delta\boldsymbol{U}_e^{(i)} + \boldsymbol{B}^T\boldsymbol{D}_p(1-R)\Delta\boldsymbol{U}_e^{(i)}\right)|\boldsymbol{J}|\,\mathrm{d}\xi\,\mathrm{d}\eta\end{aligned} \tag{8}$$

where $R$ denotes the ratio of the displacement increment concerned to the elastic stress increment to that of the total increment.

By differentiating Eq. (8) with respect to the design variable $b$, we get the sensitivity expression of the internal force vector at the transition point as

$$\frac{\partial \boldsymbol{R}^{(i)}}{\partial b} = \sum_e \int_{-1}^{1}\int_{-1}^{1}\left[\left(\frac{\partial \boldsymbol{B}^T}{\partial b}\Delta\sigma + \boldsymbol{B}^T\frac{\partial\Delta\sigma}{\partial b} + \frac{\dot{R}}{R}\boldsymbol{B}^T\Delta\sigma_e - \frac{\dot{R}}{1-R}\boldsymbol{B}^T\Delta\sigma_p\right)|\boldsymbol{J}| + \boldsymbol{B}^T\Delta\sigma\frac{\partial|\boldsymbol{J}|}{\partial b}\right]\mathrm{d}\xi\,\mathrm{d}\eta \tag{9}$$

where $\dot{R} = \partial R/\partial b$, and the derivative of stress increment in the second term has to be evaluated from

$$\frac{\partial\Delta\sigma}{\partial b} = \frac{\partial \boldsymbol{D}_p}{\partial b}\boldsymbol{B}\Delta\boldsymbol{U}_e^{(i)} + \boldsymbol{D}_e R\left(\frac{\partial \boldsymbol{B}}{\partial b}\Delta\boldsymbol{U}_e^{(i)} + \boldsymbol{B}\frac{\partial\Delta\boldsymbol{U}_e^{(i)}}{\partial b}\right) + \boldsymbol{D}_p(1-R)\left(\frac{\partial \boldsymbol{B}}{\partial b}\Delta\boldsymbol{U}_e^{(i)} + \boldsymbol{B}\frac{\partial\Delta\boldsymbol{U}_e^{(i)}}{\partial b}\right) \tag{10}$$

The derivative form of the elastic stress increment ratio $R$ is derived by differentiating the total stress expression and the yielding function [Eq. (5)]. When we denote the total stress vector at the yielding point as $\sigma = \sigma_0 + R\boldsymbol{D}_e\boldsymbol{B}\Delta\boldsymbol{U}^{(i)}$, where $\sigma_0$ is the total elastic stress vector accumulated by the incremental stress until the previous loading step, the derivative form of Eq. (10) is combined with the derivative form of the yielding function as

$$\dot{R} = -\frac{\boldsymbol{c}^T(\partial\sigma_0/\partial b + \partial\Delta\sigma_e/\partial b) - 2\sigma_Y H'\partial\bar{\varepsilon}_p/\partial b}{\boldsymbol{c}^T\Delta\sigma_e}R \tag{11}$$

The vector $\boldsymbol{c}$ is a coefficient vector of derivative form of yielding function given as

$$\boldsymbol{c}^T = (2\sigma_x - \sigma_y,\ 2\sigma_y - \sigma_x,\ 6\tau_{xy}) \tag{12}$$

For the unloading process from the plastic to elastic state, Eqs. (9) and (11) are modified with the elastic stress ratio $R = 1$. We can also treat the reloading process the same way as in Eq. (9).

The sensitivity equation (6) of displacement increment has to be solved at each Newton–Raphson iteration. Then, the total sensitivity of displacement at a load level is accumulated as

$$\frac{\partial\Delta\boldsymbol{U}^{(i)}}{\partial b} = \frac{\partial\Delta\boldsymbol{U}^{(i-1)}}{\partial b} + \frac{\partial\Delta\boldsymbol{u}^{(i)}}{\partial b} \tag{13}$$

Using these sensitivities, the design sensitivities of other response quantities such as the stress, buckling load are calculated.

## Numerical Examples

### Sensitivity Analysis of Circular Plate with a Hole

A circular plate of outer radius $b$ with a concentric hole of inner radius $a$ under internal pressure $p$ is considered. The design sensitivity analysis and the shape optimization are implemented when the outer radius $b$ is taken as the design variable. The material properties of Young's modulus, Poisson's ratio, the initial yield stress, and the strain hardening modulus are assumed, respectively, to be $E = 196$ GPa, $\nu = 0.3$, $\sigma_{Y0} = 235$ MPa, and $E_T = 4.9$ GPa. Because of symmetry, a quarter region of the circular plate is subdivided into 12 8-node quadratic elements and 51 nodes. Six loading steps of $\Delta p_1 = 8p_0$, $\Delta p_2 = \Delta p_3 = \Delta p_4 = \Delta p_5 = \Delta p_6 = 2p_0$, where the incremental pressure $p_0 = 9.8$ MPa, are applied, and a total pressure of $18p_0$ is finally loaded.

Table 1 shows the von Mises stress sensitivities on the radial axis at the first, third, and fifth loading steps in comparison with those by the finite difference method with $\Delta b/b = 0.01$. We found that, after the third loading step, the stresses near the inner surface yield, and the sensitivity discontinuity can be calculated precisely. The direct sensitivity values agree well with the finite difference values. A minimum weight design subject to the von Mises stress constraint of $\sigma_a = 255$ MPa at the inner surface is also sought for the design variable of outer radius $b$. Table 2 shows the optimization process. It is natural that the final design of $b_{opt}/a = 1.923$ is smaller than the elastic solution $b/a = 2.646$ for the same elastic allowable stress.

### Hole Shape Optimization in a Plate

The sensitivity analysis technique is also applied to determine a hole shape in a plate under small strain but plastic stress field. Figure 1 shows the design model of a square plate ($W/L = 1$) with an elliptical hole of semiaxes $a$, $b$ under uniaxial pressure loading $p = 10p_0$, where the incremental pressure $p_0 = 9.8$ MPa. The material properties of Young's modulus, Poisson's ratio, the initial yield stress, and the strain hardening modulus are assumed, respectively, to be $E = 205.8$ GPa, $\nu = 0.3$, $\sigma_{Y0} = 157$ MPa, and $E_T = 4.9$ GPa. Because of symmetry, a quarter region of the plate is

**Table 1 von Mises stress sensitivities of circular plate**

| Loading step | Radius $r/a$ | Direct differentiation method, MPa/mm | Finite difference method, MPa/mm |
|---|---|---|---|
| 1 | 1.02 | −0.6927 | −0.6924 |
| | 1.08 | −0.7942 | −0.7938 |
| | 1.14 | −0.8618 | −0.8619 |
| | 1.26 | −0.9091 | −0.9094 |
| | 1.36 | −0.9051 | −0.9050 |
| | 1.54 | −0.8620 | −0.8620 |
| | 1.69 | −0.8088 | −0.8088 |
| | 1.92 | −0.7255 | −0.7255 |
| 3 | 1.02 | −0.03695 | −0.04165 |
| | 1.08 | −0.04047 | −0.03234 |
| | 1.14 | −1.5092 | −1.5102 |
| | 1.26 | −1.5562 | −1.5572 |
| | 1.36 | −1.5317 | −1.5317 |
| | 1.54 | −1.4347 | −1.4357 |
| | 1.69 | −1.3348 | −1.3348 |
| | 1.92 | −1.1887 | −1.1887 |
| 5 | 1.02 | −0.1515 | −0.1485 |
| | 1.08 | −0.1472 | −0.1485 |
| | 1.14 | −0.1349 | −0.1367 |
| | 1.26 | −0.1135 | −0.1130 |
| | 1.36 | −0.1115 | −0.1103 |
| | 1.54 | −3.6632 | −3.6515 |
| | 1.69 | −3.2938 | −3.2703 |
| | 1.92 | −2.8322 | −2.7930 |

**Table 2 Optimization process of circular plate**

| Iteration step | Design variable $b/a$ | Maximum stress $\sigma/\sigma_a$ | Objective function $f/f_0$ |
|---|---|---|---|
| 0 | 2.000 | 0.9665 | 1.0000 |
| 1 | 1.687 | 1.3859 | 0.6156 |
| 2 | 1.884 | 1.0560 | 0.8494 |
| 3 | 1.922 | 1.0009 | 0.8985 |
| 4 | 1.923 | 1.0000 | 0.8993 |

**Table 3 Comparison of objective function, design variable, and constraint values**

| Parameter | Initial | Optimal |
|---|---|---|
| Objective function $f/W^2$ | 0.8743 | 0.8509 |
| Design variable | | |
| $a/W$ | 0.400 | 0.336 |
| $b/W$ | 0.400 | 0.565 |
| Constraint $\sigma_e/\sigma_a$ | | |
| $g_1$ | 0.8886 | 0.9940 |
| $g_2$ | 0.3022 | 0.6452 |
| $g_3$ | 1.0695 | 1.0086 |

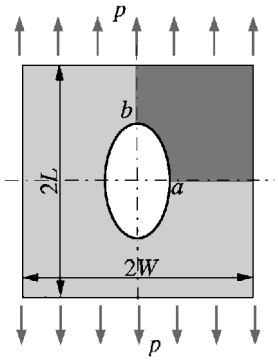


**Fig. 1 Plate with an elliptical hole under uniaxial tension.**

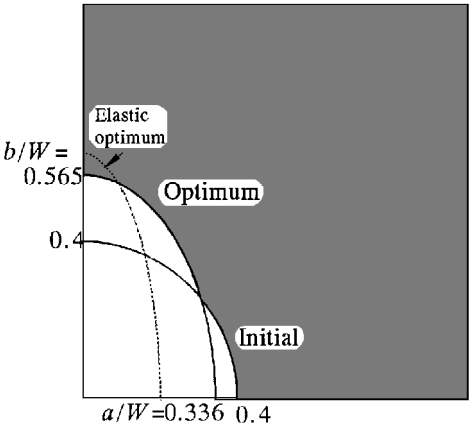


**Fig. 2 Initial and optimum shapes of elliptical holes.**

subdivided into 48 8-node quadratic elements and 173 nodes. The finite element mesh in all regions is adjusted adaptively at each optimization step. Eight loading steps of $\Delta p_1 = 3p_0$, $\Delta p_2 = \Delta p_3 = \Delta p_4 = \Delta p_5 = \Delta p_6 = \Delta p_7 = \Delta p_8 = p_0$ are applied incrementally.

The hole shape is interpolated by trigonometric function as $x_1 = a\cos\theta$ and $x_2 = b\sin\theta$, and the major and minor semiaxes $a$ and $b$ are taken as the design variables. The equivalent values of the von Mises stress on the hole boundary are restricted less than the allowable stress $\sigma_a/\sigma_{Y0} = 1.25$, and the stress constraints are imposed at several points on the boundary. To minimize the weight, the direct Taylor series approximation technique is adopted for constructing a quadratic subproblem. The approximated subproblem with move limit is solved by the complementary pivot method. The optimum solution of the design variables, the objective function, and the stress constraints obtained after seven iterations are tabulated in Table 3 in comparison with the initial values. The stress constraints at $\theta = 0$ deg ($g_1$) and 90 deg ($g_3$) are active in the optimum shape. Figure 2 shows the initial and optimum shapes of the hole. The optimum hole shape of the elastic design with same allowable stress is also shown as a reference. The optimum hole shape of elastic design ($b/a = 3.10$) is smaller and more slender than that of the plastic design ($b/a = 1.68$).

## Concluding Remarks

An exact and direct sensitivity analysis technique of the elastoplastic material governed by bilinear constitutive law, which has the discontinuous sensitivities at the yielding point, has been suggested. The sensitivity analysis technique was applied to the two-dimensional sensitivity analysis and shape optimization of the elastoplastic material. From these numerical results, it was found that 1) the sensitivity analysis technique suggested here can exactly treat the discontinuity caused by the bilinear constitutive law of elastoplastic material, and 2) the sensitivity analysis technique can effectively determine the optimum shape of an elastoplastic two-dimensional body with the aid of the approximation method.

## References

[1] Kaneko, I., and Majer, G., "Optimal Design of Plastic Structures Under Displacement Constraints," *Computer Methods in Applied Mechanics and Engineering*, Vol. 27, 1981, pp. 369–391.

[2] Ryu, Y. S., Haririan, M., Wu, C. C., and Arora, J. S., "Structural Design Sensitivity Analysis of Nonlinear Response," *Computers and Structures*, Vol. 21, Nos. 1/2, 1985, pp. 245–255.

[3] Cardoso, J. B., and Arora, J. S., "Variational Method for Design Sensitivity Analysis in Nonlinear Structural Mechanics," *AIAA Journal*, Vol. 26, No. 5, 1988, pp. 595–603.

[4] Arora, J. S., Lee, T. H., and Kumar, V., "Design Sensitivity Analysis of Nonlinear Structures—III: Shape Variation of Viscoplastic Structures," *Structural Optimization: Status and Promise*, edited by M. P. Kamat, AIAA, Washington, DC, 1993, pp. 447–485.

[5] Cheng, G. D., and Song, L., "Computational Aspects of Sensitivity Analysis of Nonlinear Discrete Structures," *Report of Institute of Mechanical Engineering*, No. 34, Aalborg Univ., Denmark, 1991.

[6] Jao, S. Y., and Arora, J. S., "Design Optimization of Non-Linear Structures with Rate-Dependent and Rate-Independent Constitutive Models," *International Journal for Numerical Methods in Engineering*, Vol. 36, No. 16, 1993, pp. 2805–2823.

[7] Ohsaki, M., and Arora, J. S., "Design Sensitivity Analysis of Elastoplastic Structures," *International Journal for Numerical Methods in Engineering*, Vol. 37, No. 2, 1994, pp. 737–762.

[8] Hisada, T., "Basic Formulation for Elastic–Plastic Stochastic Finite Element Method (Sensitivity Analysis of Nonlinear FEM)," *Transactions of Japanese Society of Mechanical Engineers*, Vol. 56, No. 524, 1990, pp. 966–970 (in Japanese).

A. D. Belegundu
*Associate Editor*

# Interaction Region of Turbulent Expansion-Corner Flow

K. Chung*
*National Cheng Kung University,*
*Tainan 70101, Taiwan, Republic of China*

## Introduction

THE Prandtl–Meyer solution for the flow around an expansion corner is well known. However, the study of Adamson[1] indicated that the transport properties in the expansion process of a real flow may have strong effects on the laminar flow properties. The velocity and streamline patterns change, and the surface pressure decreases gradually along the streamwise direction. The flow would reach the final equilibrium condition only after some finite distance downstream of the corner. The previous studies[2–6] at Mach 1.76–8.0 indicated the similar trend of the expansion process. Further, Lu and Chung[6] found that the downstream influence ($x_D/\delta_o$) of turbulent flow past expansion corners can be scaled with the hypersonic similarity parameter ($K = M_\infty\alpha$) (Fig. 1). The surface pressure of weak expansions reaches the downstream inviscid value more quickly. However, Narasimha and Sreenivasan[7] mentioned that the interaction region appears to be insensitive to the corner deflection angle for supersonic flow. In this Note, Narasimha and Sreenivasan's statement is corroborated for a low supersonic Mach number in conjunction with the work of Lu and Chung,[6] which allows conclusions to be drawn concerning Mach number effects on

Received Oct. 20, 1997; revision received March 9, 1998; accepted for publication March 9, 1998. 

*Associate Researcher, Aerospace Science and Technology Research Center, 198 Hsin-Sheng Street, Kueijen. Senior Member AIAA.